

Temperature and pressure dependent Mott potentials and their influence on self-limiting oxide film growth

Na Cai, Guangwen Zhou, Kathrin Müller, and David E. Starr

Citation: *Appl. Phys. Lett.* **101**, 171605 (2012); doi: 10.1063/1.4764552

View online: <http://dx.doi.org/10.1063/1.4764552>

View Table of Contents: <http://apl.aip.org/resource/1/APPLAB/v101/i17>

Published by the [American Institute of Physics](#).

Related Articles

Scaling of equivalent oxide thickness of atomic layer deposited HfO₂ film using RuO₂ electrodes suppressing the dielectric dead-layer effect

Appl. Phys. Lett. **101**, 172910 (2012)

Ordered graphene strips onto polymer backing prepared by laser scanning

Appl. Phys. Lett. **101**, 173102 (2012)

Properties of low indium content Al incorporated IZO (indium zinc oxide) deposited at room temperature

J. Appl. Phys. **112**, 083709 (2012)

Thin film growth by deposition of randomly shaped clusters

J. Chem. Phys. **137**, 154703 (2012)

Study of Nb epitaxial growth on Cu(111) at sub-monolayer level

J. Appl. Phys. **112**, 074328 (2012)

Additional information on *Appl. Phys. Lett.*

Journal Homepage: <http://apl.aip.org/>

Journal Information: http://apl.aip.org/about/about_the_journal

Top downloads: http://apl.aip.org/features/most_downloaded

Information for Authors: <http://apl.aip.org/authors>

ADVERTISEMENT

Universal charged-particle detector
for interdisciplinary applications:

- > Non-scanning Mass Spectrometry
- > Non-scanning Ion Mobility Spectrometry
- > Non-scanning Electron Spectroscopy
- > Direct microchannel plate readout
- > Thermal ion motion and mobility studies
- > Bio-molecular ion soft-landing profiling
- > Real-time beam current/shape tuning
- > Diagnostics tool for instrument design
- > Compact linear array for beam lines

Contact OI Analytical: +1-205-733-6900



Temperature and pressure dependent Mott potentials and their influence on self-limiting oxide film growth

Na Cai,¹ Guangwen Zhou,^{1,a)} Kathrin Müller,^{2,b)} and David E. Starr²

¹*Department of Mechanical Engineering & Multidisciplinary Program in Materials Science and Engineering, State University of New York, Binghamton, New York 13902, USA*

²*Center for Functional Nanomaterials, Brookhaven National Laboratory, Upton, New York 11973, USA*

(Received 21 July 2012; accepted 15 October 2012; published online 25 October 2012)

Classic Cabrera-Mott theory stipulates that the limited oxide-film growth results from electron tunneling from the metal through the oxide film to adsorbed oxygen. This leads to an electric field across the oxide film that assists ion migration for low-temperature oxide-film growth. Here, we show that the field-driven oxide-film growth can be manipulated via the temperature and pressure of oxidation. The magnitude of the self-generated electric field depends on the oxygen surface coverage that exhibits a Langmuir isotherm behavior with changes in temperature and oxygen pressure. These observations demonstrate the ability to tune an interfacial reaction via self-adaptation to its environment. © 2012 American Institute of Physics. [<http://dx.doi.org/10.1063/1.4764552>]

Nearly all metals form a passivating oxide film in ambient conditions. This oxide film acts as a diffusion barrier to protect the metal from further corrosion. Perhaps the most utilized description of low-temperature passivating oxide film formation is Cabrera-Mott theory.^{1,2} Since the growth of the oxide film at low temperatures (e.g., room temperature) is not thermally activated, Cabrera-Mott theory proposes that ionic diffusion through the oxide film is driven by a self-generated electric field across the oxide film. This electric field results from electron tunneling between the Fermi level of the parent metal and acceptor levels of chemisorbed oxygen at the oxide surface. The self-generated electric field reduces the energy barrier for ion migration through the oxide film, leading to rapid initial oxidation rates at low temperature. Since the tunneling current decreases exponentially with increasing oxide film thickness, the oxidation essentially stops at a limiting thickness.^{3,4}

While Cabrera-Mott theory is widely employed to understand oxide film formation at low temperatures, the validity of the theory depends critically on the assumed Mott potential, which is defined by the difference in the metal Fermi level and the chemisorbed oxygen (O-) level, $V_M = (\Phi_0 - \Phi_L)/e$, where Φ_0 is the metal work function, Φ_L is the energy difference between the vacuum level and the O-level in the adsorbed oxygen anion, and e is the elementary charge of an electron. Consequently, an electric field $-V_M/X(t)$ is set up in the oxide, where $X(t)$ is oxide thickness at the oxidation time t . The electric field provides the driving force for ion migration by effectively reducing the rate-limiting energy barrier and making low-temperature oxide film growth possible.⁵⁻¹⁰ Such a field-driven effect is quite general and critical in many interfacial reactions such as catalysis, etching, corrosion, and thin film processing at relatively low temperatures.¹¹⁻¹⁴ A central issue for the engineering of metal/oxide interfaces is understanding the formation of the Mott potential and ion transport through

the oxide film. In this work, we present experimental confirmation of the existence of the Mott potential and show that the magnitude of the Mott potential is tunable by controlling the surface coverage of adsorbed oxygen. We demonstrate that by changing the oxidation conditions (temperature and oxygen gas pressure), the self-limiting growth behavior of an oxide film can be manipulated thereby allowing control over the passivation properties of the metal surface. Our results also illustrate the more general feasibility of tuning interfacial reactions via the Mott potential and its dependence on reaction conditions.

Our experiments were carried out in an ultrahigh vacuum (UHV) chamber equipped with an x-ray photoelectron spectroscopy SPECS Phoibos 100, MCD-5 analyzer, low-energy electron diffraction (LEED), and an Ar-ion sputtering gun. The Al(111) single crystal (1-mm thick disk of 8-mm diameter) was purchased from Princeton Scientific Corp., cut to within 0.1° to the (111) crystallographic orientation and polished to a mirror finish. For the oxidation experiments at temperatures lower than 25°C , the sample was cooled by liquid-nitrogen and maintained at -50°C by counter heating with a Lakeshore 331 temperature controller. The Al surface was cleaned by cycles of Ar^+ bombardment at 25°C and annealing to 420°C . Oxygen gas (purity = 99.9999%) was introduced to the system through a variable pressure leak valve and the sample was oxidized at a specific temperature under a controlled oxygen pressure, p_{O_2} . The oxide film thickness was measured with XPS by calculating the ratio of integrated O 1s and Al 2p core level peak intensities for the initial stages of the oxidation and using the attenuation of the metallic Al(2p) peak in the oxide film for the later stages of thicker continuous oxide film growth.⁵

The clean Al(111) surface was oxidized at three different temperatures; -50°C , 25°C , and 100°C . To obtain a clear trend of the oxidation behavior, four oxygen gas pressures were examined for each temperature; $p_{\text{O}_2} = 1 \times 10^{-8}$, 10^{-7} , 10^{-6} , and 10^{-5} Torr. Fig. 1 shows the evolution of the oxide film thickness measured as a function of oxidation time extending up to approximately 5 h. For each oxygen pressure and temperature, we observe an initial rapid increase of the

^{a)}Author to whom correspondence should be addressed. Electronic mail: gzhou@binghamton.edu.

^{b)}Present address: Zernike Institute for Advanced Materials, University of Groningen, Groningen, The Netherlands.

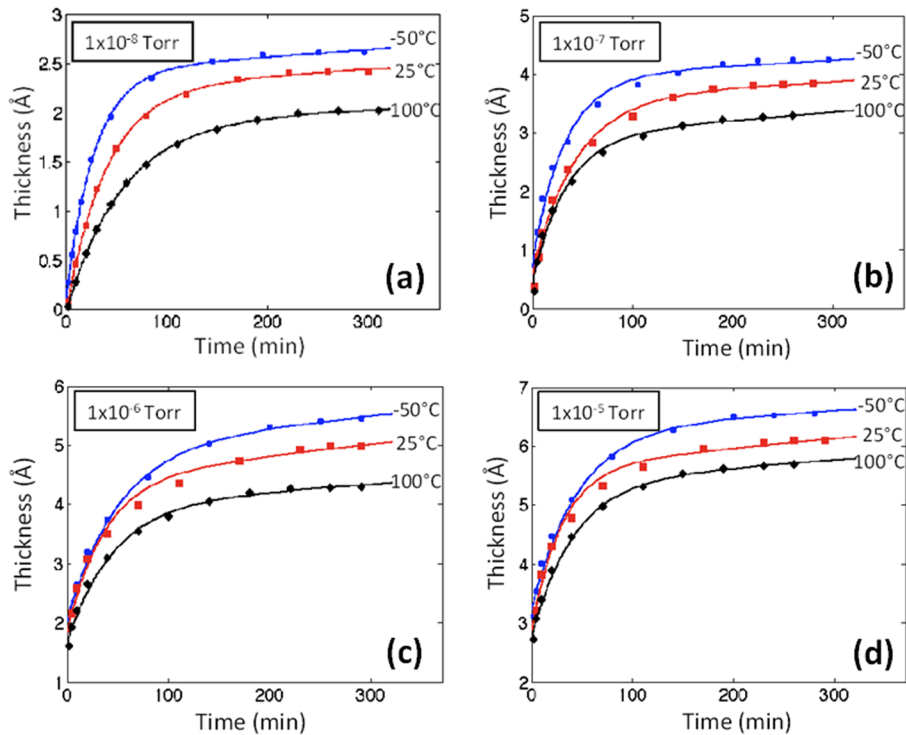


FIG. 1. Oxide film thickness as a function of time for the oxidation of Al(111) at the temperatures of -50°C , 25°C , and 100°C , and four oxygen pressures of (a) $p\text{O}_2 = 1 \times 10^{-8}$ Torr, (b) $p\text{O}_2 = 1 \times 10^{-7}$ Torr, (c) $p\text{O}_2 = 1 \times 10^{-6}$ Torr, and (d) $p\text{O}_2 = 1 \times 10^{-5}$ Torr. Superimposed on the experimental data points are theoretically computed curves based on the inverse logarithmic growth law of the Cabrera-Mott theory.

oxide film thickness, followed by a drastic reduction in the growth rate to the limited growth regime at long oxidation times. These measurements reveal the surprising result that oxidation is more rapid at lower temperature and that the self-limiting thickness of the oxide film increases with decreasing oxidation temperature. This is the case for all four oxygen gas pressures explored. Extrapolating the data in Fig. 1 to about 250 min, we obtain the effective limiting oxide-film thickness as the thickness reached when the oxide film growth rate is less than 10^{-5} Å/s (i.e., less than \sim one “oxide” ML per 10^5 s). These results are summarized in Fig. 2, where we can see that the limiting oxide-film thickness decreases with increasing oxidation temperature for a constant pressure while it increases with increasing oxygen gas pressure for a constant oxidation temperature.

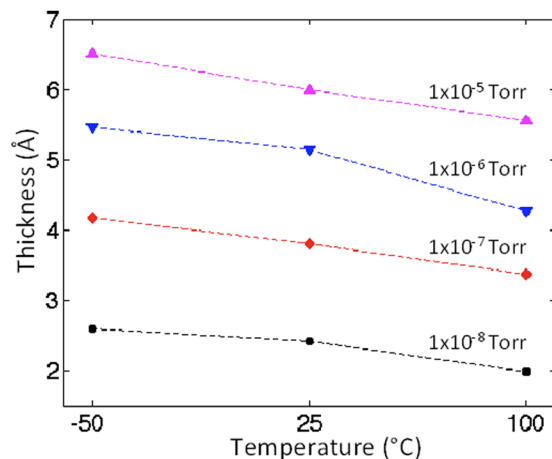


FIG. 2. Evolution of the limiting oxide-film thickness for the oxidation of Al(111) at the temperatures of -50°C , 25°C , and 100°C , and oxygen pressures of $p\text{O}_2 = 1 \times 10^{-8}$ Torr, 10^{-7} Torr, 10^{-6} Torr, and 10^{-5} Torr, respectively. The self-limiting thickness is observed to decrease with increasing the oxidation temperature for a constant oxygen pressure, while it increases with increasing oxygen gas pressure for a fixed oxidation temperature.

To further confirm such a temperature dependence of the self-limiting oxide film growth, we examined the oxide film growth kinetics by decreasing the oxidation temperature from 100°C to -50°C . As shown in Fig. 3, the clean Al(111) surface is first oxidized at $p\text{O}_2 = 1 \times 10^{-8}$ Torr and 100°C . After reaching a limiting oxide film thickness at that pressure, a stepwise increase in oxygen pressure is applied. Fig. 3 shows that additional oxide growth occurs and reaches a new limiting thickness following establishment of the limiting thickness at the lower pressure. By comparing the oxidation of the freshly cleaned Al(111) surface (Fig. 1), we note that similar limiting oxide-film thicknesses for the same oxidation conditions are reached, irrespective of whether oxidation occurs on a clean Al surface or on the surface which

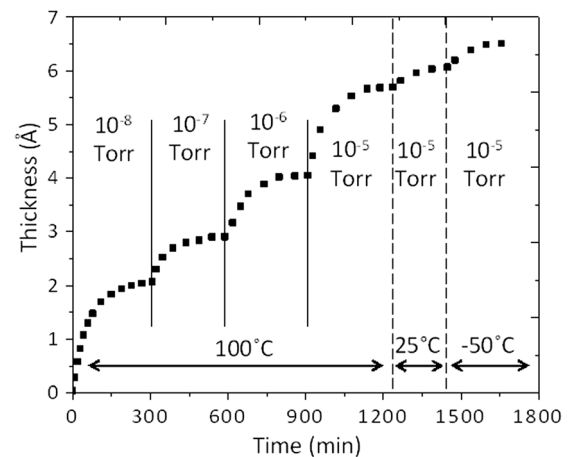


FIG. 3. Oxide film thickness evolution as a function of oxidation time and temperatures. The oxidation starts with a clean Al(111) surface at $T = 100^{\circ}\text{C}$ and $p\text{O}_2 = 1 \times 10^{-8}$ Torr. A stepwise increase in oxygen gas pressure is applied until a pressure of $p\text{O}_2 = 1 \times 10^{-5}$ Torr. Then, the sample is cooled to 25°C in $p\text{O}_2 = 1 \times 10^{-5}$ Torr, additional oxide growth occurs and a new limiting oxide-film thickness is observed. The sample is then cooled to -50°C in $p\text{O}_2 = 1 \times 10^{-5}$ Torr, resulting in an increased limiting film thickness.

is covered with a pre-existing oxide layer formed at a lower pressure.

After the limiting thickness of the oxide film is reached at $p_{\text{O}_2} = 1 \times 10^{-5}$ Torr and 100°C , the sample is cooled down to 25°C under vacuum and then oxidized at the same pressure of $p_{\text{O}_2} = 1 \times 10^{-5}$ Torr. Additional oxide growth occurs on the pre-existing, limiting-thickness oxide film grown at 100°C , resulting in a larger limiting thickness at 25°C . Once no further changes in oxide thickness are detected, the sample temperature is then lowered to -50°C , while still maintaining the same oxygen pressure. Further oxide film growth occurs and a new, larger limiting thickness is observed again. The two new limiting oxide film thicknesses obtained by cooling the sample to 25°C and -50°C are nearly the same as the limiting thicknesses of the oxide films formed from the oxidation of freshly cleaned Al surface at the two temperatures in $p_{\text{O}_2} = 1 \times 10^{-5}$ Torr. This further demonstrates the important role of temperature in determining the limiting thickness of the oxide film at a constant oxygen gas pressure.

The increase in the limiting oxide-film thickness with decreasing oxidation temperature demonstrates that oxide growth is apparently not a thermally activated process in the temperature range explored here which would result in thicker oxide films with increasing temperatures. But the thermally activated oxide growth was observed for the oxidation at 200°C which results in a thicker limiting oxide-film thickness than the lower temperatures, and this is in line with other observations.^{15,16} The self-limiting behavior of the oxide film growth, we observe for the temperature range from -50°C to 100°C , is consistent with the Cabrera-Mott model of the electric-field driven oxide growth, which predicts an inverse logarithmic growth law. The oxide films formed from the oxidation of Al at these temperatures are amorphous in nature,¹⁷⁻¹⁹ which is also confirmed by LEED in our experiments. These amorphous oxide films exhibit a deficiency of Al cations (as compared to $\gamma\text{-Al}_2\text{O}_3$) and can be described by a close packing of oxygen anions with the Al cations distributed over the octahedral and tetrahedral interstitial sites.²⁰⁻²³ The oxide film growth is thus limited by ionic migration of cations under the influence of the electric

field $E = -V_M/X(t)$ due to the Mott potential V_M across the oxide film and the rate of oxide growth follows,^{1,16}

$$\frac{dX(t)}{dt} = \Omega n \nu \exp\left(\frac{-U + qaV_M/X(t)}{kT}\right), \quad (1)$$

where $X(t)$ denotes the thickness of the oxide film at the oxidation time t , Ω is the volume of oxide formed per ion, q the charge on the migrating ions, a the interatomic jump distance, ν attempt frequency for ion migration, k the Boltzmann constant, T the temperature, and U the diffusion barrier for ion migration. Superimposed on the experimental data points in Fig. 1 is the theoretically fitted growth curves based on the inverse logarithm law given by Eq. (1) and the values of $\Omega = 0.233 \text{ nm}^3$,²⁴ $\nu = 10^{12} \text{ s}^{-1}$,^{1,24,25} and $q = 3e$ (the elementary charge $e = 1.6022 \times 10^{-19} \text{ C}$), which shows that the Cabrera-Mott growth curves agree well with the data.

The Mott potential V_M and activation energy barrier U can be evaluated from the curve fitting. Fig. 4(a) shows the values of the Mott potential V_M obtained from the fitting with the experimental data. It can be seen that V_M bears a strong dependence on the oxidation temperature and oxygen gas pressure, i.e., V_M increases with decreasing oxidation temperature for a constant oxygen pressure. We note that the activation energy barrier U for ion diffusion is nearly constant at $U = 1.5 \text{ eV}$ for the different temperatures and oxygen pressures, suggesting a similar atomic structure in the amorphous oxide films. This is supported by similar integrated Al/O peak intensity ratios of the oxide films formed at different temperatures and oxygen pressures, which give a stoichiometry of $\text{Al}_{2-x}\text{O}_3$ with $x \approx 0.24$. This also confirms that the oxide films are Al cation deficient, for which the outward diffusion of Al cations is favored over the inward diffusion of oxygen anions for oxide film growth.^{16,26}

The strong dependence of the limiting oxide-film thickness on oxidation temperature and pressure is in contrast to the behavior expected for cation-diffusion-controlled oxide film growth under the assumption of a pressure and temperature independent Mott potential. To understand the temperature and oxygen pressure dependence of the Mott potential,

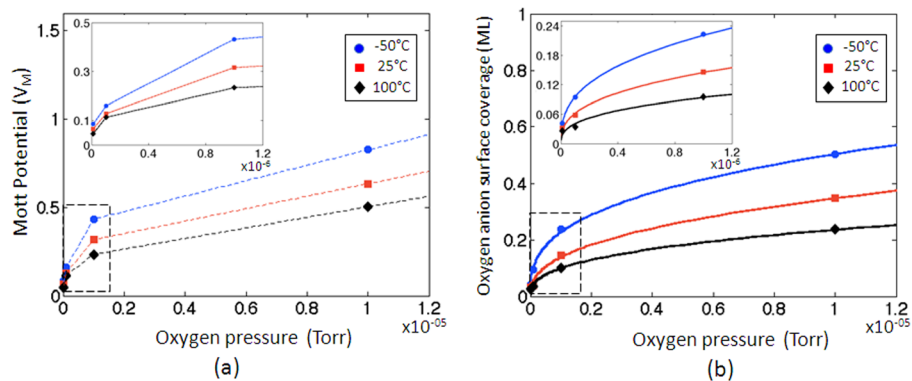


FIG. 4. (a) The actual value of the Mott potential V_M shows a strong dependence on the oxidation temperature and oxygen pressure. The magnitude of V_M decreases with temperature for a constant oxygen pressure, while it increases with increasing the oxygen pressure for a fixed temperature (dashed lines are a guide to the eye). (b) Equilibrium oxygen surface coverage with respect to the oxygen pressure for the three temperatures. The solid line corresponds to a fitting to the Langmuir isotherm for dissociative oxygen adsorption. The equilibrium surface coverage of adsorbed oxygen decreases with increasing the temperature for a constant oxygen pressure, while it increases with increasing oxygen pressure for a fixed temperature. The insets show zoomed-in view of the low oxygen pressure regime indicated by the dashed box.

we calculated the equilibrium number density, N , of chemisorbed oxygen anions on the oxide surface at the different oxidation temperatures. A parallel plate capacitor model can be used to calculate the Mott potential. The charge on the two plates is formed by electron tunneling from the oxide/metal interface to adsorbed oxygen atoms on the oxide surface. N is related to the Mott potential V_M via $N = \frac{V_M \epsilon_0 \kappa}{X_L e}$, as given by Gauss' theorem for a field between parallel plates,²⁷ where ϵ_0 is electric constant in vacuum, κ is the relative permittivity and can be taken equal to $\kappa = 9.6$,²⁸ and X_L is the limiting thickness of the oxide film. The values for the density N and, therefore, the surface coverage Θ , using the density of Al in the Al(111) surface as the reference surface, of adsorbed oxygen for different temperatures are determined and given in Fig. 4(b). It can be seen that the calculated oxygen surface coverage increases with decreasing oxidation temperature and that this is confirmed for oxidation at the four different oxygen gas pressures.

Whereas the Mott potential V_M defined by work function difference between the metal and the adsorbed oxygen does not contain any explicit temperature and oxygen pressure dependence, here we find that the actual self-generated potential V_M is temperature and pressure dependent due to the differences in the adsorbed oxygen coverage with temperature and pressure. The dependence of the equilibrium oxygen coverage on the oxygen pressure pO_2 can be described by the Langmuir isotherm for dissociative gas adsorption, $\theta = \frac{\sqrt{b(pO_2)}}{1 + \sqrt{b(pO_2)}}$

with $b = v_{des} \sqrt{2\pi m k} * \exp\{-(\Delta E_{ad} - \Delta E_{des})/kT\} * T^{-1/2}$, where T is temperature, and v_{des} denotes the pre-exponential or frequency factor, ΔE_{ad} and ΔE_{des} are the activation energies for adsorption and desorption, respectively.²⁸ The Langmuir isotherm predicts that the equilibrium oxygen coverage increases with increasing gas pressure for a constant surface temperature, whereas it decreases with increasing surface temperature for a constant gas pressure. As shown in Fig. 4(b), the determined oxygen coverage can be fitted with a Langmuir isotherm as a function of the oxygen pressure for the different oxidation temperatures. From this plot, it becomes clear that the underlying cause of the temperature and oxygen pressure dependence of the self-limiting growth of oxide films is related to the Mott potential's dependence on the oxygen surface coverage. The Mott potential increases with increasing adsorbed oxygen, leading to increased ion migration through the oxide film. Since with decreasing oxidation temperatures, the oxygen surface coverage increases, a larger Mott potential develops and, as a result, a larger limiting thickness of the oxide film is reached for a constant oxygen pressure.

In conclusion, we have studied the self-limiting growth of aluminum oxide films on an Al(111) surface under a given set of oxidation conditions. We observe that the limiting thickness of the oxide film increases with decreasing oxidation temperature over a wide range of oxygen pressures. The obtained values of the Mott potential are found to correlate with the oxygen anion coverage which can be well-described by a Langmuir isotherm dependence on the oxygen pressure and oxidation temperature. Our results reveal that temperature and gas pressure can be employed to modify the Mott

potential via changes in the oxygen surface coverage, thereby controlling the self-limiting growth of the oxide film. The overall picture of these results is that the self-generated electric field, and thus the field-assisted growth, is adjustable via controlling oxidation conditions. In principle, any atoms or molecules with an electron affinity large enough to establish the electric field across a thin oxide layer should be a candidate for a field assisted diffusion and growth process. Clearly, this might have a significant impact on the design of materials for a wide range of practical applications such as heterogeneous catalysis and thin film devices, where electrical field-driven interfacial phenomena are more dominant than thermally activated processes at relatively low temperatures.

We acknowledge support from the National Science Foundation Grant No. CBET-0932814. Research carried out in part at the Center for Functional Nanomaterials, Brookhaven National Laboratory, which is supported by the U.S. Department of Energy, Office of Basic Energy Sciences, under Contract No. DE-AC02-98CH10886.

- ¹N. Cabrera and N. F. Mott, *Rep. Prog. Phys.* **12**, 163 (1949).
- ²A. T. J. Fromhold, *Fundamental Theory of Metal Oxidation* (North-Holland, Amsterdam, 1976).
- ³A. T. Fromhold and E. L. Cook, *Phys. Rev.* **163**, 650 (1967).
- ⁴A. Szokefalvi-Nagy and E. Fromm, *Philos. Mag. Lett.* **79**, 289 (1999).
- ⁵N. Cai, G. W. Zhou, K. Muller, and D. E. Starr, *Phys. Rev. Lett.* **107**, 035502 (2011).
- ⁶N. Cai, G. W. Zhou, K. Muller, and D. E. Starr, *Phys. Rev. B* **84**, 125445 (2011).
- ⁷S. K. R. S. Sankaranarayanan, E. Kaxiras, and S. Ramanathan, *Phys. Rev. Lett.* **102**, 095504 (2009).
- ⁸V. Zhukov, I. Popova, V. Fomenko, and J. T. Yates, *Surf. Sci.* **441**, 240 (1999).
- ⁹I. Popova, V. Zhukov, and J. T. Yates, *Phys. Rev. Lett.* **89**, 276101 (2002).
- ¹⁰V. Zhukov, I. Popova, and J. T. Yates, *Phys. Rev. B* **65**, 195409 (2002).
- ¹¹Q. Fu and T. Wagner, *Surf. Sci. Rep.* **62**, 431 (2007).
- ¹²J. Hoffmann, S. Schauerermann, J. Hartmann, V. P. Zhdanov, B. Kasemo, J. Libuda, and H. J. Freund, *Chem. Phys. Lett.* **354**, 403 (2002).
- ¹³X. Yu, B. Yang, J. A. Boscoboinik, S. Shaikhutdinov, and H. J. Freund, *Appl. Phys. Lett.* **100**, 151608 (2012).
- ¹⁴B. Hoex, J. Schmidt, R. Bock, P. P. Altermatt, M. C. M. van de Sanden, and W. M. M. Kessels, *Appl. Phys. Lett.* **91**, 112107 (2007).
- ¹⁵F. Reichel, L. P. H. Jeurgens, and E. J. Mittemeijer, *Acta Mater.* **56**, 2897 (2008).
- ¹⁶L. P. H. Jeurgens, W. G. Sloof, F. D. Tichelaar, and E. J. Mittemeijer, *J. Appl. Phys.* **92**, 1649 (2002).
- ¹⁷F. Reichel, L. P. H. Jeurgens, G. Richter, and J. Mittemeijer, *J. Appl. Phys.* **103**, 093515 (2008).
- ¹⁸P. E. Doherty and R. S. Davis, *J. Appl. Phys.* **34**, 619 (1963).
- ¹⁹F. Reichel, L. P. H. Jeurgens, and E. J. Mittemeijer, *Acta Mater.* **56**, 659 (2008).
- ²⁰L. P. H. Jeurgens, W. G. Sloof, F. D. Tichelaar, and E. J. Mittemeijer, *Surf. Sci.* **506**, 313 (2002).
- ²¹L. P. H. Jeurgens, W. G. Sloof, F. D. Tichelaar, and E. J. Mittemeijer, *Thin Solid Films* **418**, 89 (2002).
- ²²A. Hasnaoui, O. Politano, J. M. Salazar, and G. Aral, *Phys. Rev. B* **73**, 035427 (2006).
- ²³P. C. Snijders, L. P. H. Jeurgens, and W. G. Sloof, *Surf. Sci.* **496**, 97 (2002).
- ²⁴L. P. H. Jeurgens, W. G. Sloof, F. D. Tichelaar, and E. J. Mittemeijer, *Phys. Rev. B* **62**, 4707 (2000).
- ²⁵P. C. J. Graat, M. A. J. Somers, A. M. Vredenberg, and E. J. Mittemeijer, *J. Appl. Phys.* **82**, 1416 (1997).
- ²⁶C. Ocal, S. Ferrer, and N. Garcia, *Surf. Sci.* **163**, 335 (1985).
- ²⁷F. P. Fehlner, *Low-Temperature Oxidation* (John Wiley & Sons, Inc., New York, 1986).
- ²⁸K. S. Shamala, L. C. S. Murthy, and K. N. Rao, *Mater. Sci. Eng., B* **106**, 269 (2004).